New age constraints on metamorphism, metasomatism, and gold mineralisation at Plutonic Gold Mine, Marymia Inlier, Western Australia

Journal:	*Australian Journal of Earth Sciences*
Manuscript ID	TAJE-RES-2015-0083.R2
Manuscript Type:	Research Paper
Date Submitted by the Author:	29-May-2016
Complete List of Authors:	Gazley, Michael; CSIRO, CESRE Vry, Julie; Victoria University of Wellington, SGEES Millet, Marc-Alban; Cardiff University School of Earth and Ocean Sciences Handler, Monica; Victoria University of Wellington, SGEES du Plessis, Ettienne; Barrick (Australia Pacific) Limited, Porgera Gold Mine Baker, Joel; The University of Auckland, School of Environment
Keywords:	Proterozoic, greenstone-hosted gold, geochronology, Pb isotope model ages, Rb-Sr ages, Capricorn Orogeny

New age constraints on metamorphism, metasomatism, and gold mineralisation at Plutonic Gold Mine, Marymia Inlier, Western Australia

M. F. Gazley[a,b], J. K. Vry[b], M.-A. Millet[c], M. R. Handler[b], E. du Plessis[d] and J. A. Baker[e]

[a]CSIRO Mineral Resources, ARRC, PO Box 1130, Bentley, WA 6102, Australia

[b]Victoria University of Wellington, PO Box 600, Wellington, New Zealand

[c]School of Earth and Ocean Sciences, Cardiff University, Cardiff CF10 3AT, United Kingdom

[d]Barrick (Australia Pacific) Limited, 6/621 Coronation Drive, Toowong, Qld 4069, Australia

[e]School of Environment, The University of Auckland, Auckland, New Zealand

Corresponding author: Michael.gazley@csiro.au

Editorial handling: A. E. Webster

Received 8 July 2015; accepted 4 July 2016

Abstract

The Plutonic Well Greenstone Belt (PWGB) is located in the Marymia Inlier between the Yilgarn and Pilbara cratons in Western Australia, and hosts a series of major Au deposits. The main episode of Au mineralisation in the PWGB was previously interpreted to have either accompanied, or shortly followed, peak metamorphism in the late Archean at ca 2650 Ma with a later, minor, event associated with the Capricorn Orogeny. Here we present new Pb isotope model ages for sulfides and Rb–Sr ages for mica, as well as a new ^{207}Pb–^{206}Pb age for titanite for samples from the Plutonic Gold Mine (Plutonic) at the southern end of the PWGB. The majority of the sulfides record Proterozoic Pb isotope model ages (2300–2100 Ma), constraining a significant Au mineralising event at Plutonic occurred >300 Ma later than previously thought. A Rb–Sr age of 2296 ± 99 Ma from muscovite in an Au-bearing sample records resetting or closure of the Rb–Sr system in muscovite at about the same time. A younger Rb–Sr age of 1779 ± 46 Ma from biotite from the same sample may record further cooling, or resetting during a late-stage episode of metasomatism in the PWGB. This could have been associated with the 1820–1770 Ma Capricorn Orogeny, or a late-stage hydrothermal event potentially constrained by a new ^{207}Pb–^{206}Pb age of 1725 ± 26 Ma for titanite in a chlorite–carbonate vein. This titanite age correlates with a pre-existing age for a metasomatic event dated at 1719 ± 14 Ma by U–Pb ages of zircon overgrowths in a sample from the Marymia Deposit. Based on the Pb-isotope data presented here, Au mineralising events in the PWGB are inferred to have occurred at ca 2630, 2300–2100 Ma, during the Glenburgh and Capricorn orogenies, and 1730–1660 Ma. The 2300–2100 Ma event, which appears to have been significant, based on the amount of sulfide of this age, correlates with the inferred age for rifting of the Marymia Inlier from the northern margin of the

Yilgarn Craton. The texturally-later visible Au may have been deposited during the Glenburgh and Capricorn orogenies.

Keywords: Proterozoic gold mineralisation; greenstone-hosted gold; geochronology; Pb isotope model ages; Capricorn Orogeny.

Introduction

One of the most significant episodes of Au mineralisation in the Yilgarn Craton (Figure 1) is recorded at ca 2650 Ma (2670–2600 Ma; e.g., Groves et al., 2000), including the richly mineralised Eastern Goldfields (ca 2640 Ma; e.g., Vielreicher, Groves, Snee, Fletcher, & McNaughton, 2010), as well as in parts of the Marymia Inlier (ca 2650 Ma; Vielreicher & McNaughton, 2002). Previously, the major episode of Au mineralisation in the Plutonic Well Greenstone Belt (PWGB) of the Marymia Inlier (Figure 1) was interpreted to have taken place at about the same time as elsewhere in the Yilgarn Craton, specifically the Eastern Goldfields (e.g., McMillan, 1996; Rowe, Awan, McCuaig, Sauter, & Vickery, 2002; Vickery, 2004). That interpretation was based on geochronological data from the Plutonic Gold Mine (Plutonic) and the wider Marymia Inlier (McMillan, 1996; Vickery, 2004; Vielreicher & McNaughton, 2002; Vielreicher, Ridley, & Groves, 2002), but included very little data that might specifically constrain the timing of Au mineralisation at Plutonic. Here we present fourteen Pb isotope model ages for pyrrhotite, arsenopyrite, pyrite and sphalerite, and two new Rb–Sr ages for muscovite and biotite, all from Au-bearing samples from Plutonic, as well as a Pb–Pb age for titanite from a late-stage chlorite vein. Our results suggest that a significant Au mineralisation event took place at 2300–2100 Ma and, although the host rocks at Plutonic are Archean in age, that the majority of Au mineralisation occurred during the Paleoproterozoic. These ages also provide new constraints on cooling after peak metamorphism and late-stage metasomatic events at Plutonic. The significance of Paleoproterozoic ages for Au mineralisation on the margins of the Yilgarn Craton was recently highlighted as Doyle et al. (2015) report Au mineralisation at the Tropicana deposit at ca 2520 Ma, while Kirland et al. (2015) report ca 2100 Ma ages for Au mineralisation in the Albany-Fraser Orogen (SE Yilgarn Craton).

Geological setting

Plutonic has a total endowment of ~10.5 million ounces of Au (Fallon, Porwal, & Guj, 2010), and is located ~800 km northeast of Perth, Western Australia (Figure 1). The Marymia Inlier is an Archean basement high located between the Pilbara and Yilgarn cratons and is surrounded by Proterozoic rocks. Dentith et al. (2014) argue that rift architecture preserved along the northern margin of the Yilgarn Craton suggests that the Marymia Inlier separated from the Eastern Goldfields Superterrane of the Yilgarn Craton during continental rifting and deposition of the Windplain Group of the Yerrida Basin (Figure 1), possibly at ca 2170 Ma (Woodhead & Hergt, 1997). The inlier was uplifted during the Paleoproterozoic Capricorn Orogeny (ca 1820–1770 Ma) (e.g., Occhipinti, Sheppard, Nelson, Myers, & Tyler, 1998a; Occhipinti, Swager, & Pirajno, 1998b; Pirajno, Jones, Hocking, & Halilovic, 2004; Tyler & Thorne, 1990). The PWGB is a NE–SW-trending, ~50 km long, ~10 km wide granite–greenstone terrane in the Marymia Inlier. The southern end of the PWGB is significantly more structurally

complex than the northern end of the inlier; with significant structural complexity occurring late in its tectonic history (Duclaux, Hough, Gazley, & de Beer, 2011; Duclaux, Hough, & Gazley, 2012).

Based on U–Pb sensitive high resolution ion microprobe (SHRIMP) analyses of zircon from samples collected both at Plutonic and farther northeast in the belt, peak amphibolite-facies metamorphism in the PWGB is dated at 2660–2630 Ma (McMillan, 1996; Vickery, 2004; Vielreicher & McNaughton, 2002). The main Au mineralising event was interpreted to have accompanied or shortly followed peak metamorphism in the PWGB (McMillan, 1996; Rowe, Awan, McCuaig, Sauter, & Vickery, 2002; Vickery, 2004; Vielreicher et al., 2002), although there is no geochronological evidence from Plutonic to support this. The available data from Plutonic showed Pb isotope model ages of ca 2100 Ma for pyrite in samples that were not associated with Au (Vielreicher et al., 2002), with ca 1730–1660 Ma ages obtained from galena (McMillan, 1996; Vielreicher et al., 2002), both at Plutonic and elsewhere in the PWGB.

Known economic concentrations of Au at Plutonic occur mainly within the Mine Mafic Package, which is predominantly comprised of amphibolite-facies metabasaltic rocks that are typically high Fe- to high Mg-tholeiite in composition (Gazley, 2011; Morgan, 2004). Minor and thin (typically < 1 m) discontinuous units within the metabasalt sequence include the metamorphosed equivalents of silica- and sulfide-rich sediments, and rock types that are interpreted as having been derived from sediments with relatively mafic bulk compositions. These minor rock types can be interlayered on a cm- to dm-scale. The metabasaltic rocks preserve pillow structures in low-strain areas, demonstrating that deposition of the Mine Mafic Package occurred in a subaqueous environment. Granitoid plutons surrounding the greenstone belt are dated at ca 2720 Ma (U–Pb dating of zircons; Vielreicher & McNaughton, 2002), and appear to have been overthrust onto the generally NE-dipping greenstone sequence. The entire sequence is cross-cut by at least two generations of sub-vertical dolerite dykes (Gazley, Tutt, Brisbout, Fisher, & Duclaux, 2014a). Based on U–Pb dating of zircons from a narrow, cross-cutting felsic porphyry, deposition of the volcano-sedimentary package occurred before 2680 Ma (McMillan, 1996; Vickery, 2004).

The Mine Mafic Package varies in thickness from <20 to >300 m, and is for the most part overturned (e.g., Gazley, Vry, du Plessis, & Handler, 2011a). Evidence for overturning of the Mine Mafic Package can be found in komatiitic textures in the ultramafic rocks that overlie and underlie the Mine Mafic Package, and variation in elemental concentrations in sections through the Mine Mafic Package (Gazley, 2011; Gazley et al., 2011a; Vickery, 2004). Recently compiled geochemical cross-sections through the Mine Mafic Package show that there is no significant structural duplication of the package within the current mine workings (Gazley, 2011; Gazley et al., 2011a, 2012).

Peak metamorphic conditions were ~8 ± 2 kbar and ~600 ± 50°C (Gazley, Vry, & Boorman, 2011b; Gazley, Vry, & Pearce, 2014b), based on results of both hornblende–plagioclase geothermobarometry and petrological forward modelling using the computer programs THERMOCALC (revised version of Powell & Holland, 1988) and Theriak/Domino (de Capitani & Brown, 1987; de Capitani & Petrakakis, 2010). The metamorphism formed hornblende–plagioclase–titanite–quartz–epidote assemblages in the mafic rocks (Gazley et al., 2011b). Prograde ilmenite and rare traces of rutile can be preserved in titanite, whereas prograde actinolite and cummingtonite can be preserved in the cores of hornblende, and variable amounts of carbonate, chlorite and epidote were introduced during retrogression. The development of these textures is consistent with their formation in a single, major metamorphic episode that reached amphibolite-facies conditions in the Plutonic area.

Gold mineralisation

Gold mineralisation is typically confined to well-defined, narrow (1–3 m wide), biotite-bearing lodes, commonly referred to as "brown lodes" (Vickery, 2004), which are sub-parallel to the dominant foliation within the Mine Mafic Package and tend to be near-parallel to the original stratigraphy as marked by the rare metasedimentary horizons (Bagas, 1998, 1999). Representative underground and polished hand sample photographs are presented in Figure 2. The Au lodes are localised into a north-trending zone ca 1 km wide and 3 km long. In the north of the deposit, drag on a large thrust fault has folded the Mine Mafic Package to create an upright limb in an otherwise overturned sequence. A series of large, steep, normal faults that trend northeast cross-cuts the deposit, offset Au-bearing lodes by up to a few tens of metres. These faults do not appear to be a dominant control on Au mineralisation, although local increases in Au grade are evident in their vicinity, with visible Au commonly observed.

Brown lodes (Figure 2a–d) contain Au in association with quartz–biotite–amphibole–titanite–epidote–carbonate–tourmaline–arsenopyrite–pyrrhotite ± chalcopyrite ± scheelite. Brown lodes are typically siliceous, very fine-grained, and laminated on a sub-mm scale; biotite tends to define a foliation parallel to the laminations. In overall appearance, the brown lode can resemble a metamorphosed banded chert (Figures 2c), with individual laminae differing in the proportions and grain sizes of biotite, quartz and sulfides, and in the nature of the sulfide minerals present. Arsenopyrite is typically the dominant sulfide, though in some lodes, pyrrhotite is dominant. The arsenopyrite is preferentially situated in fine-grained, quartz-rich laminae, and is generally too fine-grained to separate from the rock for analysis. Arsenopyrite crystals are for the most part euhedral and not strongly oriented. Blebs of visible Au are common and appear to be associated with both calc-silicate alteration, and chloritisation of biotite, which overprint the earlier fabrics and at least one generation of arsenopyrite (Duclaux et al., 2013; Gazley, Duclaux, Fisher, Hough, & Pearce, 2015; Pearce et al., 2015). Pyrrhotite can be texturally later than the arsenopyrite (Figure 3a,c). Large-scale geochemical datasets show that Au/As varies widely across the deposit, but that generally Au is strongly associated with As (Gazley et al., 2012, 2014c).

Other styles of Au mineralisation are also present at Plutonic in lesser amounts. These include shear-hosted lodes, rare muscovite-rich lodes (Figure 2f), and low- to marginally-economic Au grades that are associated with the late-stage quartz–carbonate ± pyrrhotite ± chalcopyrite ± sphalerite ± galena that infills some faults.

Sample descriptions

MG801: This sample is of an early quartz–tourmaline–arsenopyrite–Au vein. The Au is concentrated near the edges of the vein and infills fractures that cross-cut the tourmaline. Some of the arsenopyrite appears to be texturally later than the vein as a coarse, early, generation of arsenopyrite was cross-cut by later arsenopyrite with quartz veining and abundant visible Au (Duclaux et al., 2013).

MG034: This sample is of muscovite-rich lode that is rare within the deposit (Figure 2f); grades of 15–30 g/t are common for this mineralisation style. The rock is dominated by very fine-grained crenulated matrix of green muscovite, with lesser amounts of arsenopyrite, biotite, tourmaline and rare, late pyrrhotite. The arsenopyrite crystals have a random habit, and tend to grow in clusters that

radiate out from a central point and overprint the pre-existing crenulation. Visible Au is present as <10 µm blebs on the margins of arsenopyrite grains or as inclusions within it (Figure 3a).

MG233: This sample is of brown lode, but the sulfide mineral assemblage is pyrrhotite-dominated (quartz–biotite–chlorite–amphibole–titanite–epidote–pyrrhotite ± arsenopyrite ± chalcopyrite ± scheelite ± Au; Figure 3f). The fine laminations that characterise typical brown lode are lacking, and there is comparatively more textural evidence of deformation, in the form of a fabric defined by biotite that wraps around the pyrrhotite crystals, in places forming biotite and chlorite wings on pyrrhotite. Amphiboles are early and over-printed by the sulfide, mica and Au (similar to textures in sample MG222; Figure 3c), and chloritisation of biotite is common (see lower centre of Figure 3f). Gold (~400 g/t in this sample) is common as small blebs up to several hundred microns across, both disseminated within the calc-silicate groundmass and along the edges of pyrrhotite crystals.

MG354: This sample is of a thin (mm-scale), late-stage, chlorite–carbonate vein with calcite crystals that have their largest dimensions (up to ~1 cm) in the plane of the vein. This vein is undeformed and cross-cuts all other features and fabrics. Euhedral to subhedral titanite crystals in this vein are pale pink to orange in colour and up to ~3 mm in length. No sulfides or Au are present in this sample.

MG039: This sample is of metamorphosed ultramafic rock located close to the contact between the metabasaltic Mine Mafic Package and the overlying ultramafic rocks (Figure 3b). Large dravite crystals and massive pyrrhotite are not uncommon on the contact, and in this sample are associated with low Au grades of ~2 g/t. The sample consists primarily of acicular actinolite, with Fe-rich chlorite, talc, and minor feldspar and calcite.

MG025/MG201: Both these samples are from a quartz–pyrrhotite–chalcopyrite ± carbonate ± Au vein from within the Bintang Fault zone, which is confined to the Mine Mafic Package in the northern part of the deposit. The fault zone (up to several metres wide) generally dips to the northwest at ~50°, and has strike and dip lengths on the order of 100s of metres. It is interpreted to have formed during the Capricorn Orogeny by Vickery (2004). The average Au grade of this structure is ~4.3 g/t.

MG800: This sample is of a quartz–carbonate–galena–sphalerite ± Au vein that infills dilational zones in a large fault in the northeast of the deposit. Outside of sparse occurrences in metasedimentary units, this fault (and associated splays) is the only occurrence of galena or sphalerite in the deposit. The fault is near-vertical and dips towards the WNW; it has km-scale strike continuity through the deposit. Low Au grades are locally associated with this fault.

MG218/MG340: These two samples come from small, flat-lying (<30° dip) quartz–carbonate–pyrrhotite–chalcopyrite ± Au veins. Carbonate is more abundant than quartz.

MG802: In this sample, Au is intergrown with pyrite in a quartz–pyrite vein that cross-cuts a cherty brown lode. This is a very rare style of Au mineralisation at Plutonic, as pyrite is uncommon and seldom associated with Au. Figure 2e shows late-stage Au associated with carbonate over-printing a cherty brown lode from a few metres further along the lode from where this sample was collected. Pyrrhotite as the dominant sulfide in the brown lode while pyrite is absent there.

MG222/MG224: These two samples are of the brown lode mineralisation (e.g. Figure 2d), that occurs in an overturned limb of the Mine Mafic Package where deformation is more pervasive, and the package is thinner than elsewhere in the deposit. Both samples consist mainly of quartz, carbonate

and amphibole, but are overprinted by abundant epidote and chlorite, with lesser biotite, and very rare titanite (e.g. Figure 3c, d). Pyrrhotite is the dominant sulfide, and arsenopyrite is very rare. The pyrrhotite and Au are late-stage as they overprint the texturally early amphibole crystals.

Methods

Electron microprobe

Electron probe microanalyses (EPMA) were obtained using wavelength-dispersive methods at Victoria University of Wellington, New Zealand, using a JEOL JXA-733 SuperProbe. The accelerating voltage was 15 kV, and the sample current was 12 nA. Spot sizes of 1–20 µm were utilised depending on the volatile and/or alkali content of the mineral being analysed and the grain size. Back-scatter electron (BSE) images of samples were collected for identification of zoned sulfides, while biotite was analysed to determine its phlogopite composition.

Scanning electron microscopy

Energy dispersive spectroscopy (EDS) elemental maps were collected using a Phillips XL40 scanning electron microscope (SEM) at the Australian Resources Research Centre, Perth, Australia. The resulting maps are a combination of the BSE image (showing variations in atomic mass) and EDS signal. This method provides a high-spatial resolution map of the elemental variation in the mapped area.

Rb–Sr dating of biotite and muscovite

Mica-bearing rock samples were lightly crushed in a steel percussion mortar, sieved, and 15–70 mg separates of biotite and muscovite were hand-picked for acid digestion. Whole rock samples were ground in a tungsten carbide TEMA ring mill until fine and a 50–60 mg sub-sample was digested. The mica separates and whole rock powders were digested using HF–HNO_3 acid at 120°C in 7 mL Savillex™ Teflon™ beakers. After complete dissolution, each sample was taken up in 3 M HNO_3, and a 0.2 mL aliquot was taken for $^{87}Rb/^{86}Sr$ ratio determinations. The Sr was separated from the remaining solution using 3 M HNO_3 on ~5 mm Sr-SPEC™ resin beds in columns made from 1 mL Eppendorf™ pipette tips. Rb/Sr ratios were measured on an Agilent™ 7500cs inductively coupled plasma mass spectrometer (ICP-MS) using a 1 ppb 1:1 Rb:Sr solution as a standard. $^{87}Sr/^{86}Sr$ ratios were measured relative to SRM 987 using a Nu Plasma multi-collector (MC-)ICP-MS at Victoria University of Wellington (VUW), New Zealand. Standard reference materials BHVO-2 and BCR-2 were processed through the same sample preparation as the unknown samples and yielded $^{87}Sr/^{86}Sr = 0.703467 \pm 0.000008$ and $^{87}Sr/^{86}Sr = 0.705029 \pm 0.000008$, respectively, which are in excellent agreement with reference values for BHVO-2 of $^{87}Sr/^{86}Sr = 0.703467 \pm 0.000017$ and for BCR-2 of $^{87}Sr/^{86}Sr = 0.705000 \pm 0.000030$ (Jochum et al., 2005).

Pb–Pb dating of titanite

Titanite was analysed in situ using laser ablation ICP-MS at VUW, New Zealand. A rock chip containing titanite was mounted in epoxy with a shard of the homogeneous glass reference standard NIST610, and the surface prepared by grinding using wet 400–4000 µm grit SiC paper, followed by successive lap polishing using 3 and 1 µm diamond suspensions. The titanite crystals were analysed using an Agilent 7500cs ICP-MS coupled to a New Wave 193 nm (deep UV) solid-state laser ablation system. The titanite was ablated with a static laser beam (35 µm diameter) at 5 Hz and 65% power,

with analyses acquired over ~30 s, or until the laser had ablated through the crystal. The reference Pb isotope data of Baker, Peate, Waight, & Meyzen (2004) for the NIST610 standard were used to correct the raw titanite Pb isotopic data for instrumental mass bias. Glass standard analyses bracketed every five sample analyses. The magnitude of the mass bias correction was typically 0.35% per atomic mass unit and instrumental mass bias typically drifted <<0.05% per atomic mass unit between standard analyses. Typical internal precisions for the $^{206}Pb/^{204}Pb$ and $^{207}Pb/^{206}Pb$ ratios were ±5% and ±0.5% (2 se), respectively. Lead isotopic data for the titanite samples were corrected for common Pb using the measured ^{204}Pb counts and a common Pb composition of $^{206}Pb/^{204}Pb = 15.5$ and $^{207}Pb/^{204}Pb = 15.5$ (Cumming & Richards, 1975). The final calculated age is the mean of the individual $^{207}Pb/^{206}Pb$ ages calculated for the five most radiogenic titanite analyses. The uncertainty quoted on this age is the two standard deviation of the five individual $^{207}Pb/^{206}Pb$ ages and, in principle, includes all of the potential sources of error quoted above (i.e. mass bias correction, common Pb correction and internal errors on the Pb isotope ratios).

Pb isotope model ages

Samples selected for Pb-isotope analyses came in one of two forms, either thin-section billets, where the corresponding thin-section could be examined to ensure there was no zonation within the sulfide minerals, or polished blocks, in which the sulfides were examined *in situ* using BSE techniques to ensure there was no zonation. In the case of the thin-section billets, the billet was crushed for picking, while in the case of polished blocks, the block was crushed; for those samples that were not entirely consumed in this process, SEM EDS maps are presented in Figure 3. Samples weighing 7–55 mg of either arsenopyrite or pyrrhotite were hand-picked under a binocular microscope from crushed samples. Separates were dissolved with HBr, HF and HNO_3 in 7 mL Savillex™ Teflon™ beakers. Lead was separated from each solution using conventional HCl–HBr anion exchange procedure. Lead isotope ratios were measured on a Nu Plasma MC-ICP-MS at VUW, New Zealand, by sample–standard bracketing with SRM981. To document the reproducibility of measurements, SRM981 was analysed five times at the start of each analytical session. The average of these SRM981 analyses was $^{208}Pb/^{204}Pb = 36.7216 \pm 0.0027$, $^{207}Pb/^{204}Pb = 15.4988 \pm 0.0011$, and $^{206}Pb/^{204}Pb = 16.9402 \pm 0.0011$, which are in excellent agreement with reference values of $^{208}Pb/^{204}Pb = 36.7262 \pm 0.0031$, $^{207}Pb/^{204}Pb = 15.5000 \pm 0.0013$, $^{206}Pb/^{204}Pb = 16.9416 \pm 0.0013$ (Baker et al., 2004). Error correlations with respect to Pb isotope data were not considered, given that the uncertainties associated with the model ages are orders of magnitude larger. Varying the Pb isotope ratios for the oldest model ages (ca 2630 Ma) by the reported error (<0.05%) results in a variation in the model age of ca 30 kyr, which is negligible compared to the ± 50 Ma error ascribed to Pb isotope model ages in this study.

For those samples for which there was sufficient material available, U/Pb ratios were also measured. Separates were dissolved with HF, HNO_3 and HCl in 7 mL Savillex™ Teflon™ beakers. Uranium and Pb concentrations were measured on a Thermo Scientific Element2 sector-field ICP-MS, at VUW, New Zealand. The data were calibrated using BHVO-2, at four dilutions to create a calibration curve across the concentration range. The reported errors include propagated analytical uncertainties from the standard calibration and from the sample analysis.

Results

New Rb–Sr age data for biotite and muscovite separates and whole rock powders are presented in Table 1 from an Au-bearing sample (MG034), from which Pb isotope model ages for sulfides were

also obtained (Table 2; U–Pb data, Table 3). A three-point isochron age of 2296 ± 99 Ma was obtained from two muscovite separates and the whole rock. This approach takes advantage of inter-crystal variations in mica Rb/Sr ratios to calculate ages and, although it is possible that these could be due to small inclusions of other minerals such as apatite within the mica samples that would affect the measured Rb/Sr ratios, none were observed during BSE imaging and EPMA of the biotite (phlogopite, Mg / (Mg + Fe_T) = 0.77–0.79). The two-point biotite–whole rock isochron yielded an age of 1779 ± 46 Ma.

Pb isotopic data yields a calculated $^{207}Pb/^{206}Pb$ age for five most radiogenic titanite crystals from sample MG354 (Table 4) of 1725 ± 26 Ma. This age has a reasonably strong common Pb correction that may affect its reliability; however, it closely correlates with a pre-existing age for a metasomatic event dated at 1719 ± 14 Ma by U–Pb ages of zircon overgrowths in a sample from the Marymia Deposit in the north of the PWGB (Vielreicher & McNaughton, 2002).

Pb isotope model ages for ten pyrrhotite, three arsenopyrite, one sphalerite, and one pyrite separate(s) are presented in Table 2 and Figure 4. $^{207}Pb/^{206}Pb$ model ages are calculated using the Cumming & Richards (1975) Model III for $t_{7/6}$ ages, with Stacey & Kramers (1975) model ages for the same samples presented for comparison. Three groups of Cumming & Richards (1975) model ages were obtained; the oldest grouping from five pyrrhotite–bearing, one arsenopyrite-bearing and one pyrite-bearing sample(s) at ca 2300–2100 Ma, with later ages at ca 1960 Ma, ca 1830 Ma and ca 1730–1660 Ma (Table 2). In addition, an early, coarse arsenopyrite crystal in a quartz vein (sample MG801), yields a model age of 2628 Ma. The sulfides from all the samples analysed have uniformly low U/Pb with the highest value of 0.02 being recorded for MG233 (Table 3). These low U/Pb mean that the Pb isotope model ages presented in Table 2 likely represent ages of crystallisation and are unaffected by radiogenic Pb produced from U decay.

Discussion

Dating methods that do not directly analyse an Au-bearing phase rely on geological field evidence such as cross-cutting relationships and petrographic textural evidence to support the argument that the mineral that was dated grew or was isotopically reset at the time of Au mineralisation. At Plutonic, Au is not texturally associated with commonly used silicate or phosphate geochronometers, but instead typically occurs in textural equilibrium with sulfides (e.g. pyrrhotite, Figure 3c, d, f), or contained within them (e.g. arsenopyrite).

Peak metamorphic conditions

The results of U–Pb dating of zircon have constrained the timing of peak metamorphism within the PWGB at 2660–2630 Ma (McMillan, 1996; Vielreicher & McNaughton, 2002 (belt-wide); Vickery, 2004 (Plutonic area)). This is consistent with the timing of metamorphism in the Yilgarn Craton (e.g., Czarnota et al., 2010; Goscombe, Blewett, Czarnota, Groenewald, & Mass, 2009; Groves et al., 2000). We identified no minerals or mineral assemblages that would enable to further constrain the timing of this major metamorphic episode.

Temperatures

At Plutonic the maximum peak metamorphic temperatures were ~600°C, based on hornblende–plagioclase geothermobarometry and phase equilibria modelling (Gazley et al., 2011b, 2014b). This is

higher than the closure temperatures (T_c) for the Rb–Sr system in micas, so the Rb–Sr ages will record cooling or resetting following the metamorphic peak. Depending on grain size, muscovite has a closure temperature of 500–550°C (Willigers, Mezger, & Baker, 2004). As the muscovite within the studied sample is rather fine grained (~200 µm), it is probable that the closure temperatures were at the lower end of this range, and that the temperature at 2296 ± 99 Ma was ~500°C. The closure temperature for the Rb–Sr system in biotite (~400–450°C) is sensitive to both grain size and composition, with higher phlogopite ($Mg/(Mg + Fe_T)$) contents being associated with higher closure temperatures (Vry & Baker, 2006; Willigers et al., 2004). As the biotite in MG034 is very fine-grained and has an $Mg / (Mg + Fe_T) = 0.77–0.79$, the biotite age of 1779 ± 46 Ma most likely represents closure of the Rb–Sr system during cooling through ~400°C.

Our new Rb–Sr ages may be indicative of slow cooling from peak temperatures of ~600°C at ca 2630 Ma to ~400°C at 1779 ± 46 Ma, giving an average cooling rate of 0.23°C/Ma for ca 850 Ma. This is an extremely slow cooling rate (cf. rates in slow-cooled, deep crustal granulites of ≤ 1–2°C/Ma; e.g., Ashwal, Tucker, & Zinner, 1999). The rocks could have remained buried until exhumed by a later event, such as the Paleoproterozoic orogenies that affected the PWGB (Glenburgh 2005–1950 Ma and Capricorn 1820–1770 Ma orogenies; e.g. Johnson et al., 2011, 2013; Occhipinti et al., 1998a, b; Pirajno et al., 2004; Sheppard, Bodorkos, Johnson, Wingate, & Kirkland, 2010). This interpretation is consistent with that proposed by Muhling (1988, 1990) who suggested that granulite facies metamorphism commenced in the Narryer Gneiss Complex of the northern Yilgarn Craton at ca 3300 Ma but it was not uplifted until during the formation of the Capricorn Orogen at <2000 Ma. It is also conceivable that these ages are associated with resetting of the Rb–Sr system during later metasomatism (and potentially Au mineralisation).

Timing of Au mineralisation

Ideally, a geochronometer that produced ages that were not model dependent would be used to date Au mineralisation. As discussed previously, Rb–Sr ages will record cooling, or resetting, following the peak metamorphism and are thus not ideal for constraining the age of Au mineralisation. Options for dating sulfide minerals include the Re–Os system or Pb isotopes. However, the closure temperature for the Re–Os system in sulfide minerals is, like the Rb–Sr system in biotite, at ~400–450°C (e.g., Cherniak, 2010). As such, Re–Os ages on sulfide minerals from Plutonic would likely yield ages of ca 1800 Ma, even if the sulfides crystallised near the metamorphic peak (2660–2630 Ma when temperatures were ~600°C), and would not yield meaningful insights into the timing of Au mineralisation.

Closure temperatures for U and Pb diffusion in sulfides are not known; however, major elements in sulfides, particularly in pyrrhotite, are widely regarded as being susceptible to low-temperature re-equilibration (e.g., Cherniak, 2010; Hagemann, Brown, Ridley, Stern, & Fournelle, 1998). Even so, the observation that many of the sulfide Pb isotope model ages from Plutonic cluster at ages (2300–2100 Ma) that are older than the Rb–Sr ages for biotite (T_c ~ 450–400°C; e.g., Willigers et al., 2004), suggests that the T_c for Pb diffusion in both pyrrhotite and arsenopyrite may be higher than 400°C. It is possible that the T_c for Pb diffusion in arsenopyrite is even higher, as the texturally older generation of arsenopyrite in MG801 returned a Pb isotope model age of 2628 Ma, and the inferred metamorphic temperatures at that time were ~600°C (at 2660–2630 Ma; Gazley et al., 2011b, 2014b; Vielreicher & McNaughton, 2002).

Previous studies have indicated that Pb isotope model ages for sulfides from mineral deposits compare well with those obtained using conventional geochronometers (e.g., Ho McNaughton, & Groves, 1994; McNaughton & Dahl, 1987; McNaughton & Groves, 1996). However, the age of sulfides as determined by Pb isotope model ages is highly model dependent. The Stacey and Kramers (1975) model returns ages for the oldest sulfides of ca 2800 Ma (Table 5), which are older than the probable age of the host rocks and significantly pre-date peak metamorphism. Accordingly, we prefer the model of Cumming and Richards (1975), as this model gives oldest ages that are around the age of peak metamorphism at ca 2660–2630 Ma and another age population ca 1730–1660 Ma, around the age of a metasomatic event dated by Pb–Pb and U–Pb dating at ca 1720 Ma (Vielreicher & McNaughton 2002; this study). It is interesting to note that Hawke *et al*. (2015) preferred the Stacey and Kramers (1975) model for their Pb isotope study of mineralisation at the DeGrussa Cu deposit, located ~30 km away from Plutonic, and associated mineralisation in the Proterozoic basins in the Capricorn Orogen. However, for the reasons outlined above, we consider the Cumming and Richards (1975) model to be more appropriate for the Marymia Inlier.

Given that only very minor galena and pyrite are present at Plutonic, the choice of minerals that can be analysed to constrain the timing of Au deposition is restricted. Arsenopyrite and pyrrhotite can in places reliably preserve initial Pb isotope compositions (McNaughton & Groves, 1996), even though their Pb isotope ratios may not plot on the mantle growth curve, due to the tendency of these minerals to incorporate small amounts of U and Th into their crystal structures (McNaughton, 1987). In sulfides other than galena or pyrite, the sample with the least radiogenic Pb in a suite of samples from the same mineralisation event is most likely to represent the best estimate for the initial Pb (Ho et al., 1994; McNaughton & Groves, 1996). McNaughton and Dahl (1987) showed that Pb isotope model ages for syngenetic galena and Fe-sulfides from elsewhere in the Yilgarn Craton possibly over-estimate the age of formation by up to ca 70 Ma. Addition of our samples to the data from Vielreicher *et al.* (2002), the ages derived from the projection of arrays back to the growth curve are 2666 Ma and 1773 Ma (Figure 4). These ages are consistent with the individual Pb isotope model ages for sulfide minerals of ca 2630 Ma and 1730–1660 Ma since these individual ages have an error of ± 50 Ma (Cumming & Richards, 1975).

Data from different sulfide minerals will reflect natural variations in Pb isotope ratios and subsequent re-equilibration of the sulfides, even if the sulfides all crystallised during the same event (c.f. Ho et al., 1994). Our data has been obtained from different sulfide minerals (pyrrhotite n = 9; pyrite n = 1; arsenopyrite n = 3; sphalerite n = 1), collected from within different lithologies and parts of an Au mineralising system, and so are likely to have natural variation in their Pb isotope compositions. Indeed, in sample MG034, two separates of arsenopyrite picked from the same sample yields an age of 2124 Ma and 2039 Ma, while a pyrrhotite separate from the same sample yields an age of 1919 Ma. The difference between two separates of the same mineral are 85 Ma apart and are within the ±50 Ma error we suggest is appropriate for these age determinations. The younger pyrrhotite age may reflect a lower T_c for Pb diffusion in pyrrhotite, but it is close to within error of the younger arsenopyrite age. Samples MG201 and MG025 both come from the Bintang Fault, which Vickery (2004) suggested formed during the Capricorn Orogeny (1820–1770 Ma); the ages for these samples are 1962 Ma and 1833 Ma, respectively. These ages are outside a ±50 Ma error of each other, but given the Pb-isotope heterogeneity in sample MG034 where two separates of the same mineral were picked from the same sample, the measured Pb-isotope signatures may reflect the same event. A better interpretation may be that the Bintang Fault started to form during the Glenburgh Orogeny

(2005–1950 Ma) and continued to be active during the Capricorn Orogeny (1820–1770 Ma). This Glenburgh age may also correlate to the 1919 Ma age of pyrrhotite in sample MG034.

Lead isotope data for sulfides from the PWGB are presented in Table 5 (Vielreicher et al., 2002; references therein), which help to constrain the timing of Au mineralisation. Similar to this study, Vielreicher *et al.* (2002) reported three main clusters of Pb isotope model ages in the PWGB at ca 2650, ca 2100 and ca 1730–1660 Ma. Previous studies interpreted the main Au mineralisation event at Plutonic to be syn- to slightly post-peak metamorphism (2660–2630 Ma; e.g., Rowe et al., 2002; Vickery, 2004; Vielreicher et al., 2002), although the only Pb isotope model ages of sulfides of this age that are demonstrably associated with Au mineralisation are from the Triple P and Marymia deposits >30 km north of Plutonic (e.g., Vielreicher et al., 2002). The oldest age that we derived was from an early, coarse, arsenopyrite crystal in a quartz vein (sample MG801), which yields a model age of 2628 Ma. Microtextures suggests that two generations of arsenopyrite are present and that no visible Au is associated with the older generation, where the coarse grained arsenopyrite was broken, with abundant visible Au infilling these fractures and a younger generation of arsenopyrite (Duclaux et al., 2013). The 2628 Ma for arsenopyrite is confirms there was early sulfide deposition at Plutonic at conditions close to peak metamorphism, but the textures argue that significant Au mineralisation occurred later.

The southern end of the PWGB is significantly more structurally complex than the north of the inlier; and there are structures that were active (and Au mineralised) late during the tectonic evolution of Plutonic (e.g. Duclaux et al., 2011, 2012). This late-stage structural history that is not evident at the north of the PWGB may account for the larger spread of Pb isotope model ages at Plutonic than the northern parts of the belt. The largest cluster of Pb isotope model ages for sulfides that either host or are in textural equilibrium with Au (e.g. samples MG034, MG222, MG224, MG233) are at ca 2300–2100 Ma (Tables 2). Free Au typically appears to be texturally late (Figure 3a, c–f), and thus could have been deposited during at either 2300–2100 Ma (this study) or 1730–1660 Ma (Vielreicher et al., 2002). All of the available evidence supports the interpretation that if there was an early ca 2650 Ma Au mineralisation event, it was either not strongly developed in the Plutonic region, or it was overprinted by later Au mineralisation to such an extent that a ca 2650 Ma Pb isotope signature can no longer be discerned. It is possible that an apparent age of 2300–2100 Ma could be obtained if a sulfide sample contained approximately equal proportions of sulfides that crystallised in two different events (e.g., ca 2650 and ca 1770 Ma), and if the ages from the earlier event were not reset (as indicated by the star on Figure 4). However, on the basis of observed textures, most of the samples that record the 2300–2100 Ma event only contain a single generation of sulfides, making a mixing hypothesis improbable (e.g. samples MG034, MG222, MG224, MG233; Figure 3a, c–f).

Our new results from Au-bearing samples from Plutonic predominantly record Paleoproterozoic ages at 2300–2100 Ma (Table 2). They complement and reinforce earlier evidence from Pb isotope model ages (Table 5) for pyrite from the region (McMillan, 1996; Vielreicher & McNaughton, 2002). The Paleoproterozoic ages post-date the inferred timing of amphibolite-facies peak metamorphism at ca 2660–2630 Ma by >300 Ma, and plot between a Yilgarn-like cluster of ages ca 2650 Ma, and younger ages attributable to effects of younger orogenies; the 2005–1950 Ma Glenburgh Orogeny and 1820–1770 Ma Capricorn Orogeny. Taken together, all the available evidence supports the interpretation that a major episode of Au mineralisation affected the Plutonic area and adjacent parts of the PWGB in the Paleoproterozoic. A ca 2300–2100 Ma age of Au mineralisation is consistent with the ca 2100 Ma age for Au mineralisation on the margin of the Yilgarn in the Albany-Fraser Orogen (Kirkland et

al., 2015). Significantly, Dentith et al. (2014) argue that rift architecture preserved along the northern margin of the Yilgarn Craton suggests that the Marymia Inlier separated from the Eastern Goldfields Superterrane of the Yilgarn Craton during continental rifting and deposition of the Windplain Group of the Yerrida Basin (possibly ca 2170 Ma; Woodhead & Hergt, 1997). Dentith et al. (2014) note that this was at the same time as a significant phase of Au mineralisation occurred at Plutonic based on the Pb-isotope ages presented in Gazley (2011). It is possible that the tectonism associated with the separation of the Marymia Inlier from the Yilgarn Craton was responsible for metasomatism and Au mineralisation within the Marymia Inlier itself.

A significant amount of the Au is late-stage (Figure 3f), associated with calc-silicate alteration that overprints both sulfide textures and chloritisation of biotite (e.g. Figure 3f). If the Au were early (i.e. pre-metamorphic peak) the textural association with chloritisation of biotite would not be preserved. Indeed, recent work by Pearce *et al.* (2015) argues that nanostructure in the Au grains of samples from Plutonic are consistent with very late stage deposition of the Au and post-dates any deformation. These mineralogical observations are consistent with our new geochronology.

Late-stage metasomatism

Our new $^{207}Pb/^{206}Pb$ age determination for vein-hosted titanite records an age of 1725 ± 26 Ma (Table 4). Based on the biotite Rb–Sr results (cooling through ~400°C at 1779 ± 46 Ma), the temperature of the host rock into which the chlorite–carbonate–titanite vein was emplaced was likely to be ≤ 400°C. As the T_c for Pb diffusion in titanite is considerably higher than that (~600°C; Willigers, Baker, Krogstad, & Peate, 2002), we interpret the age as dating titanite crystallisation and vein emplacement. It is likely that our titanite $^{207}Pb/^{206}Pb$ age records the same metasomatic event that was dated at 1719 ± 14 Ma by U–Pb ages of zircon overgrowths in a sample from Marymia (Vielreicher & McNaughton, 2002). Based on the strong temporal relationship between the ca 1720 Ma metasomatic event (recorded in unmineralised samples) and the 1730–1660 Ma Au mineralising event recorded by Vielreicher et al. (2002)'s Pb isotope data, it is probable both represent the same event, which was relatively widespread throughout the PWGB. The youngest Pb-isotope age that we determined was 1516 Ma from sample MG039; this sample is located on the contact between the mafic and ultramafic packages, contains massive pyrrhotite and minor Au (~2 g/t). This age supports the argument for late-stage Au mineralisation (or at least mobility) associated with fluid flow along the margin of these two units late in the tectonic history of the deposit.

Conclusions

The new geochronology data presented in this paper, coupled with previous constraints (e.g., McMillan, 1996; Vickery, 2004; Vielreicher & McNaughton, 2002; Vielreicher et al., 2002), record a geological history that is related, but intrinsically different, to other Au deposits within the PWGB and the majority of other deposits elsewhere in the Yilgarn Craton.

The rocks of the Plutonic area were affected by amphibolite-facies metamorphism at high pressures (≥ 8 kbar at ~600°C) at ca 2660–2630 Ma. Subsequently, there were a number of Au mineralisation events during a long period of cooling. The Rb–Sr data from a muscovite is that it represents a cooling age at 2296 ± 99 Ma as *T* cooled through ~500°C, and a younger biotite age at 1779 ± 46 Ma may reflect either further cooling or perturbation of the Rb–Sr isotopic system during metasomatism associated with the Capricorn Orogeny at 1820–1770 Ma. It is unclear whether this age correlates to a further metasomatic event that occurred at ca 1720 Ma as dated by both U–Pb dating of zircon

overgrowths (McMillan, 1996; Vielreicher & McNaughton, 2002), and Pb–Pb dating of titanite (this study). This metasomatic event may be associated with late-stage Au mineralisation, as the projection of arrays back to the growth curve yields Pb isotope ages for sulfides at ca 1773 Ma.

On the basis of the Pb-isotope data from Au-associated sulfides, Au mineralising events are inferred to have occurred at ca 2630, 2300–2100 Ma, during the Glenburgh and Capricorn orogenies, and 1730–1660 Ma in the PWGB. A major Au mineralising event is inferred to have occurred at 2300–2100 Ma, >300 Ma later than previously interpreted for Plutonic, the PWGB, or the Yilgarn Craton (e.g., Groves et al., 2000; McMillan, 1996; Vielreicher et al., 2002, 2010). Dentith *et al*. (2014) argue that the Marymia Inlier rifted off the northern margin of the Yilgarn Craton, separating from the Eastern Goldfields Superterrane, at ca 2170 Ma. It is possible that the tectonism associated with the separation of the Marymia Inlier from the Yilgarn Craton was responsible for metasomatism and Au mineralisation within the Marymia Inlier itself, as this corresponds to the cluster of 2300–2100 Ma Pb-isotope model ages for Au-associated sulfides at Plutonic.

Acknowledgements

This paper comprises part of MFG's PhD at Victoria University of Wellington, New Zealand. Funding for the research, and permission to publish this paper, comes from Barrick Australia Pacific Limited. Discussions with K. Cassidy, G. Duclaux, R. Hough and A. Pocock have greatly improved this manuscript. The input of G. Carr is gratefully acknowledged with respect to interpreting the Pb isotope data. We are grateful for the comprehensive reviews of N. Phillips, S. Johnson and an anonymous reviewer.

References

Ashwal, L. D., Tucker, R. D., & Zinner, E. K. (1999). Slow cooling of deep crustal granulites and Pb-loss in zircon. *Geochimica et Cosmochimica Acta, 63*, 2839–2851.

Bagas, L. (1998). Geology of the Marymia 1:100 000 sheet: Western Australia Geological Survey, 1:100 000 Geological Series Explanatory Notes, pp. 23.

Bagas, L. (1999). Early tectonic history of the Marymia Inlier and correlation with the Archaean Yilgarn Craton, Western Australia. *Australian Journal of Earth Science, 46*, 115–125.

Baker, J. A., Peate, D. W., Waight, T. E., & Meyzen, C. (2004). High-precision Pb isotopic analysis of standards and samples using thallium and a lead double spike with a double focusing MC-ICPMS. *Chemical Geology, 211*, 275–303.

Cherniak, D. J. (2010). Diffusion in carbonate, fluorite, sulfide minerals, and diamond. *Reviews in Mineralogy and Geochemistry, 72*, 871–897.

Czarnota, K., Champion, D. C., Goscombe, B., Blewett, R. S., Cassidy, K. F., Henson, P. A., Groenewald, P. B. (2010). Geodynamics of the eastern Yilgarn Craton. *Precambrian Research, 183*, 175–202.

Cumming, G. L., & Richards, J. R. (1975). Ore lead isotope ratios in a continuously changing earth. *Earth and Planetary Science Letters, 28*, 155–171.

de Capitani, C., & Brown, T. H. (1987). The computation of chemical equilibrium in complex systems containing non-ideal solutions. *Geochemica et Cosmochimica Acta, 51*, 2639–2652.

de Capitani, C., & Petrakakis, K. (2010). The computation of equilibrium assemblage diagrams with Theriak/Domino software. *American Mineralogist, 95*, 1006–1016.

Dentith, M. C., Johnson, S. P., Evans, S., Aitken, A. R. A., Joly, A., Thiel, S. & Tyler, I. M. (2014). A magnetotelluric traverse across the eastern part of the Capricorn Orogen: *Geological Survey of Western Australia, Report 135*, p. 49.

Doyle, M. G., Fletcher, I. R., Foster, J., Large, R. R., Mathur, R., McNaughton, N. J., Meffre, S., Muhling, J. R., Phillips, D. & Rasmussen, B. (2015). Geochronological Constraints on the Tropicana Gold Deposit and Albany-Fraser Orogen, Western Australia. *Economic Geology, 110*, 355–386.

Duclaux, G., Hough, R., Gazley, M. F., & de Beer, S. (2011). September. Deposit-scale characterisation of hydrothermal systems: a holistic view of gold mineralisation Plutonic Mine, Western Australia. In *Society of Geology Applied to Mineral Deposits Biennial Meeting* (p. 4).

Duclaux, G., Hough, R., & Gazley, M. F. (2012). Late tectonic evolution of Plutonic Gold Mine and controls on gold mineralisation. Structural Geology and Resources. *Australian Institute of Geoscientists Bulletin, 56*, 75–78.

Duclaux, G., Hough, R., Fisher, L., Laukamp, C., Barnes, S., Walshe, J., & leGras, M. (2013). Plutonic Gold Mine Minerals System Project report. CSIRO, Australia, pp 173.

Fallon, M., Porwal, A., & Guj, P. (2010). Prospectivity analysis of the Plutonic Marymia Greenstone Belt, Western Australia. *Ore Geology Reviews, 38*, 208–218.

Gazley, M. F. (2011). Metamorphism, geochronology and stratigraphy of an amphibolite-facies greenstone-hosted gold deposit: Plutonic Gold Mine, Marymia Inlier, Western Australia. Unpublished PhD thesis, Victoria University of Wellington, New Zealand, pp. 164.

Gazley, M. F., Vry, J. K., du Plessis, E., & Handler, M. R. (2011a). Application of hand-held X-ray fluorescence analyses to Metabasalt Stratigraphy, Plutonic Gold Mine, Western Australia. *Journal of Geochemical Exploration, 110*, 74–80.

Gazley, M. F., Vry, J. K., & Boorman, J. C. (2011b). *P–T* evolution in greenstone belt mafic amphibolites: an example from Plutonic Gold Mine, Marymia Inlier, Western Australia. *Journal of Metamorphic Geology, 25*, 685–697.

Gazley, M. F., Duclaux, G., Fisher, L. A., de Beer, S., Smith, P., Taylor, M., Swanson, R., Hough, R. M., & Cleverley, J. (2012). Improving geological and metallurgical understanding of Plutonic Gold Mine, Western Australia, using 3-D visualisation of portable X-Ray fluorescence data. *Applied Earth Science Trans. IMM B, 20*, 88–96.

Gazley, M. F., Tutt, C. M., Brisbout, L. I., Fisher, L. A., & Duclaux, G. (2014a). Application of portable X-ray fluorescence analysis to characterize dolerite dykes at Plutonic Gold Mine, Western Australia. *Geochemistry: Exploration, Environment, Analysis, 14*, 223–231.

Gazley, M. F., Vry, J. K., & Pearce, M. A. (2014b). Further evidence for ~8 kbar amphibolite facies metamorphism in the Marymia Inlier, Western Australia. *Australian Journal of Earth Science, 61*, 919–926.

Gazley, M. F., Tutt, C. M., Fisher, L. A., Latham, A. R., Duclaux, G., Taylor, M. D., & de Beer, S. J. (2014c). Objective geological logging using portable XRF geochemical multi-element data at Plutonic Gold Mine, Marymia Inlier, Western Australia. *Journal of Geochemical Exploration, 143*, 74–83.

Gazley, M. F., Duclaux, G., Fisher, L. A., Hough, R. M., & Pearce, M. (2015). High-resolution characterisation of Gold Mineralisation at Plutonic Gold Mine, Western Australia – Evidence for the late-stage deposition of high-grade gold. PACRIM 2015 Congress, Hong Kong, 18 – 21 March 2015, 51–58.

Goscombe, B., Blewett, R. S., Czarnota, K., Groenewald, P. B., & Mass, R. (2009). Metamorphic evolution and integrated terrane analysis of the Eastern Yilgarn Craton: Rationale, methods, outcomes and interpretation. Geoscience Australia, Record 2009/23, pp. 270.

Groves, D. I., Goldfarb, R. J., Knox-Robinson, C. M., Ojala, J., Gardoll, S., Yun, G. Y., & Holyland, P. (2000). Late-kinematic timing of orogenic gold deposits and significance for computer based exploration techniques with emphasis on the Yilgarn Block, Western Australia. *Ore Geology Reviews, 17*, 1–38

Hagemann, S. G., Brown, P. E., Ridley, J., Stern, P., & Fournelle, J. (1998). Ore petrology, chemistry and timing of electrum in the Archaean hypozonal Transvaal lode gold deposit, Western Australia. *Economic Geology, 93*, 271–291.

Hawke, M. L., Meffre, S., Stein, H., Hilliard, P., Large, R., & Gemmell, J. B. (2015). Geochronology of the DeGrussa volcanic-hosted massive sulphide deposit and associated mineralisation of the Yerrida, Bryah and Padbury Basins, Western Australia. *Precambrian Research, 267*, 250–284.

Ho, S. E., McNaughton, N. J., & Groves, D. I. (1994). Criteria for determining initial Pb-isotope compositions of pyrite in Archaean lode-gold deposits: a case study at Victory, Kambalda, Western Australia. *Chemical Geology, 111*, 57–84.

Jochum, K. P., Nohl, U., Herwig, K., Lammel, E., Stoll, B., & Hofmann, A. W., 2005. GeoReM: A new geochemical database for reference material and isotopic standards. *Geostandards and Geoanalytical Research* **29**, 333–338.

Johnson, S. P., Sheppard, S., Rasmussen, B., Wingate, M. T. D., Kirkland, C. L., Muhling, J.R., Fletcher, I. R. & Belousova, E. A. (2011). Two collisions, two sutures: Punctuated pre-1950Ma assembly of the West Australian Craton during the Ophthalmian and Glenburgh Orogenies. *Precambrian Research, 189*, 239–262.

Johnson, S. P., Thorne, A. M., Tyler, I. M., Korsch, R. J., Kennett, B. L. N., Cutten, H. N., Goodwin, J., Blay, O., Blewett, R. S., Joly, A. & Dentith, M. C. (2013). Crustal architecture of the Capricorn Orogen, Western Australia and associated metallogeny. *Australian Journal of Earth Sciences, 60*, 681–705.

Kirkland, C. L., Spaggiari, C. V., Smithies, R. H., Wingate, M. T. D., Belousova, E. A., Sweetapple, M. T., Watkins, R., Tessalina, S., & Creaser, R. (2015). The affinity of Archean crust on the Yilgarn-Albany-Fraser Orogen boundary: Implications for gold mineralisation in the Tropicana Zone. *Precambrian Research, 266*, 260–281.

Kretz, R. (1983). Symbols for rock-forming minerals. *American Mineralogist, 68*, 277–279.

Martin, D. McB., & Thorne, A. M. (2002). Revised lithostratigraphy of the Mesoproterozoic Bangemall Supergroup on the Edmund and Turee Creek 1:250 000 map sheets, Geological Survey of Western Australia, Record, 2002/15, pp. 27.

McMillan, N. M. (1996). Late-Archaean, syn-amphibolite facies, lode-gold deposits overprinted by Palaeoproterozoic deformation, metasomatism and hydrothermal activity at Marymia, Western Australia. PhD Dissertation University of Western Australia.

McNaughton, N. J. (1987). Lead-Isotope Systematics for Archaean Sulfide Studies. In S. E. Ho, & D. I. Groves (Eds) *Recent advances in understanding Precambrian gold deposits.* Geology Department and University Extension, University of Western Australia, Publication 11.

McNaughton, N. J., & Groves, D. I. (1996). A review of Pb-isotope constraints of the genesis of lode-gold deposits in the Yilgarn Craton, Western Australia. *Journal of the Royal Society of Western Australia, 28*, 123–129.

McNaughton, N. J., & Dahl, N. (1987). A geochronological framework for gold mineralization in the Yilgarn Block, Western Australia. In S. E. Ho & D. I. Groves (Eds) *Recent advances in*

understanding Precambrian gold deposits. Geology Department and University Extension, University of Western Australia, Publication 11.

Morgan, R. (2004). The Lithogeochemical Characteristics of the Mine Mafic Within Zone 19 (The Baltic), Plutonic Gold Mine, Western Australia. Honours Dissertation, Curtin University of Technology.

Muhling, J. R. (1988) The Early to Middle Proterozoic of Australia The nature of Proterozoic reworking of early Archaean gneisses, Mukalo Creek Area, Southern Gascoyne Province, Western Australia. *Precambrian Research, 40*, 341–362.

Muhling, J. R. (1990). The Narryer Gneiss Complex of the Yilgarn Block, Western Australia: a segment of Archaean lower crust uplifted during Proterozoic orogeny. *Journal of Metamorphic Geology, 8*, 47–64.

Occhipinti, S. A., Grey, K., Pirajno, F., Adamides, N. G., Bagas, L., Dawes, P., & Le Blanc Smith, G. (1997). Stratigraphic revision of the Palaeoproterozoic rocks of the Yerrida, Bryah and Padbury Basins (former Glengarry Basin), Geological Survey of Western Australia, Record 1997/3, pp. 56.

Occhipinti, S. A., Sheppard, S., Nelson, D. R., Myers, J. S., & Tyler, I. M. (1998a). Syntectonic granite in the southern margin of the Palaeoproterozoic Capricorn Orogen, Western Australia. *Australian Journal of Earth Sciences, 45*, 509–512.

Occhipinti, S. A., Swager, C. P., & Pirajno, F. (1998b). Structural-metamorphic evolution of the Palaeoproterozoic Bryah and Padbury Groups during the Capricorn orogeny, Western Australia. *Precambrian Research, 90*, 141–158.

Pearce, M. A., Gazley, M. F., Fisher, L. A., Saunders, M., Hough, R. M., & Kong, C. (2015). Nanoparticles are the key to forming giant orogenic gold deposits. SEG conference, Hobart, Australia.

Pirajno, F., Jones, J. A., Hocking, R. M., & Halilovic, J. (2004). Geology and tectonic evolution of Paleoproterozoic basins of the eastern Capricorn Orogen, Western Australia. *Precambrian Research, 128*, 315–342.

Powell, R., & Holland, T. J. B. (1988). An internally consistent thermodynamic dataset with uncertainties and correlations: 3: Application methods, worked examples and a computer program. *Journal of Metamorphic Geology, 6*, 173–204.

Rowe, R. J., Awan, A. W., McCuaig, T. C., Sauter, P. C., & Vickery, N. M. (2002). Structural Geology of the Plutonic Gold Mine. Applied Structural Geology for Mineral Exploration and Mining International Symposium, Kalgoorlie, WA, pp. 180–185.

Sheppard, S., Bodorkos, S., Johnson, S. P., Wingate, M. T. D., & Kirkland, C. L. (2010). *The Paleoproterozoic Capricorn Orogeny: Intracontinental reworking not continent–continent collision. Geol. Surv. West. Aust*.

Stacey, J. S., & Kramers, J. D. (1975). Approximation of the terrestrial lead isotope evolution by a two-stage model. *Earth and Planetary Science Letters, 26*, 207–221.

Steiger, R. H., & Jäger, E. (1977). Subcommission on geochronology: convention on the use of decay constants in geo- and cosmochronology. *Earth and Planetary Science Letters, 36*, 359–362.

Tyler, I. M., & Thorne, A. M. (1990). The northern margin of the Capricorn Orogen, Western Australia – an example of an early Proterozoic collision zone. *Journal of Structural Geology, 12*, 685–701.

Vickery, N. M. (2004). The Plutonic Gold Deposit, Western Australia: Geology and Geochemistry of an Archaean Orogenic Gold System. PhD Dissertation, University of New England.

Vielreicher, N. M., & McNaughton, N. J. (2002). SHRIMP U–Pb geochronology of magnetism and thermal events in the Archaean Marymia Inlier, central Western Australia. *International Journal of Earth Science, 91*, 406–432.

Vielreicher, N. M., Ridley, J. R., & Groves, D. I. (2002). Marymia: an Archaean, amphibolite facies, hosted orogenic lode-gold deposit overprinted by Paleoproterozoic orogenesis and base metal mineralization, Western Australia. *Mineralium Deposita, 37*, 737–764.

Vielreicher, N. M., Groves, D. I., Snee, L. W., Fletcher, I. R., & McNaughton, N. J. (2010). Broad synchroneity of three gold mineralization styles in the Kalgoorlie Gold Field: SHRIMP, U–Pb and $^{40}Ar/^{39}Ar$ geochronological evidence. *Economic Geology, 105*, 187–227.

Vry, J. K., & Baker, J. A. (2006). LA-MC-ICPMS Pb–Pb dating of rutile from slowly cooled granulites: Confirmation of the high closure temperature of Pb-diffusion in rutile. *Geochimica et Cosmochimica Acta, 70*, 1807–1820.

Williger, B. J. A., Baker, J. A., Krogstad, E. J., & Peate, D. (2002). Precise and accurate in situ Pb–Pb dating of apatite, sphene and monazite by laser ablation multiple-collector ICP-MS. *Geochimica et Cosmochimica Acta, 66*, 1051–1066.

Williger, B. J. A., Mezger, K., & Baker, J. A. (2004). Development of high precision Rb–Sr phlogopite and biotite geochronology: an alternative to $^{40}Ar/^{39}Ar$ mica dating? *Chemical Geology*, *213*, 339–358.

Woodhead, J. D., & Hergt, J. M. (1997). Application of the 'double spike' technique to Pb-isotope geochronology. *Chemical Geology, 138*, 311–321.

Figure and table captions

Figure 1. Simplified location and geological map for Plutonic Gold Mine modified after Gazley et al. (2014a). (a) Distribution of Archean basement rocks in Western Australia. Note the presence of a series of Archean Inliers in the Capricorn Orogen, between the large Yilgarn and Pilbara cratons. (b) Simplified geological map of the Archean Marymia Inlier, surrounding Proterozoic basins, North Yilgarn Craton, along with major mapped structures and active Au mines and deposits. The geological features have been extracted from online GSWA data (http://geodownloads.dmp.wa.gov.au/datacentre/datacentreDb.asp). Proterozoic basin ages are defined in Martin and Thorne (2002), Occhipinti et al. (1997) and Pirajno et al. (2004).

Figure 2. Representative underground and polished hand samples of mineralisation at Plutonic. (a, b) Typical brown lode in underground faces; (c) cherty lode with late-stage Au; (d) pyrrhotite-rich brown lode with abundant chlorite, (e) thin metachert with abundant late-stage Au and pyrrhotite in the more mafic wall rock, and (f) muscovite-rich green lode.

Figure 3. Representative SEM EDS maps of mineralised samples from Plutonic; mineral abbreviations after Kretz (1983); amph = amphibole. Elements included in the map as indicated. (a) MG034, muscovite-rich lode, predominantly a quartz–muscovite–arsenopyrite rock with Au associated with the boundaries of arsenopyrite grains or as inclusions therein; (b) MG039, massive pyrrhotite on the mafic–ultramafic boundary, minor chalcopyrite associated with pyrrhotite; (c–e) MG222/MG224, brown lode with late-stage pyrrhotite associated with visible Au overprinting metamorphic amphibole, Au is typically associated with biotite or calc-silicate alteration; and (f) MG233, sheared brown lode, Au is associated with pyrrhotite and may be disseminated through the quartz and calc-silicate alteration as per panel (e), biotite is commonly chloritised.

Figure 4. Concordia diagram showing $^{206}Pb/^{204}Pb$ and $^{207}Pb/^{204}Pb$ isotope ratios for sulfide minerals from the Plutonic Well Greenstone Belt from this study (MG), and Vielreicher et al. (2002) (NV). Mineral abbreviations after Kretz (1983). The grey shaded field represents Pb isotope ratios from the Peak Hill area (after Vielreicher & McNaughton, 2002, and references therein). The star indicates a theoretical Pb isotope composition derived from approximately equal proportions of sulfides that crystallised in two different events at ca 2650 and ca 1720 Ma. Location abbreviations: Marymia = Marymia Gold Mine; PPP = Triple P deposit; Plutonic = Plutonic Gold Mine.

Table 1. $^{87}Rb/^{86}Sr$ and $^{87}Sr/^{86}Sr$ ratios for biotite- and muscovite-bearing samples from Plutonic.

Table 2. Lead isotope compositions of sulfides from samples from Plutonic samples.

Table 3. Uranium and lead concentrations of sulfides from samples from Plutonic.

Table 4. Pb isotope ratios for the five most radiogenic titanite in a late-stage chlorite–carbonate vein from Plutonic.

Table 5. Lead isotope compositions of sulfides from the PWGB.

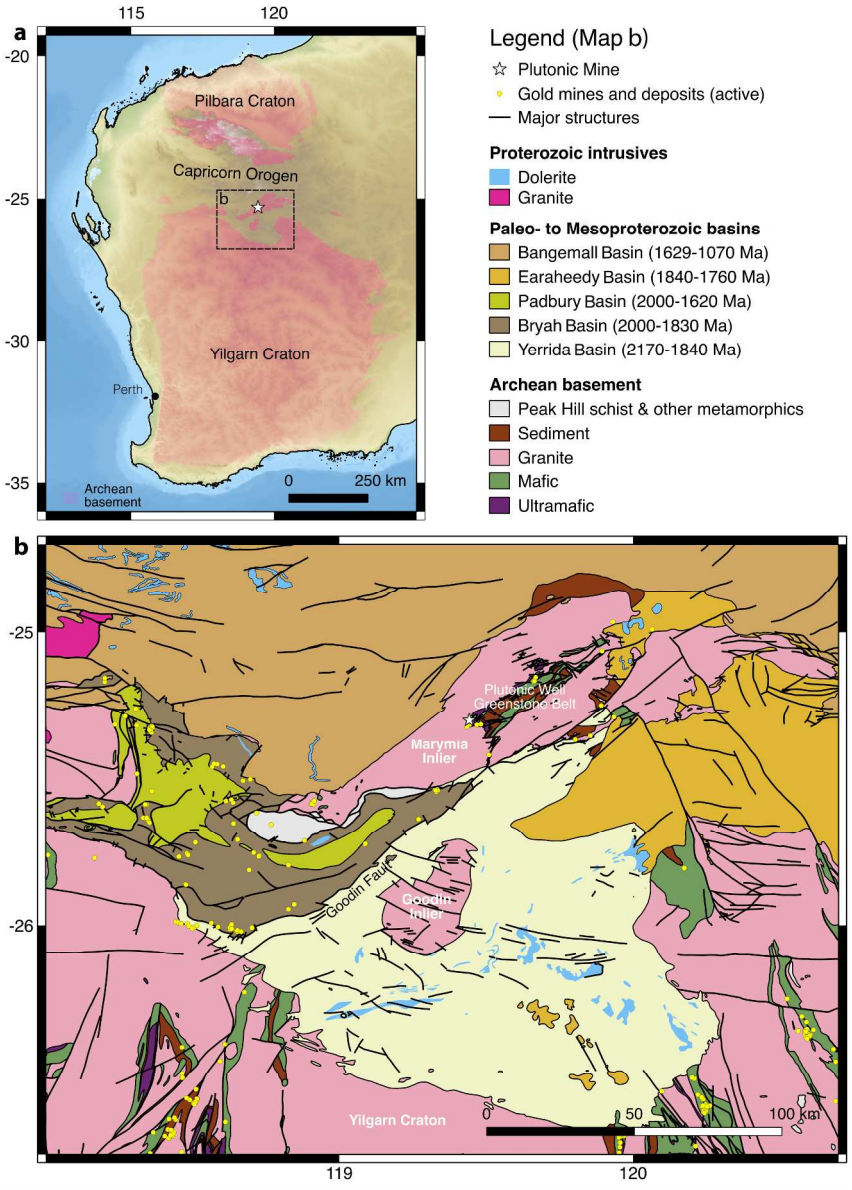

Figure 1. Simplified location and geological map for Plutonic Gold Mine modified after Gazley et al. (2014a). (a) Distribution of Archean basement rocks in Western Australia. Note the presence of a series of Archean Inliers in the Capricorn Orogen, between the large Yilgarn and Pilbara cratons. (b) Simplified geological map of the Archean Marymia Inlier, surrounding Proterozoic basins, North Yilgarn Craton, along with major mapped structures and active Au mines and deposits. The geological features have been extracted from online GSWA data (http://geodownloads.dmp.wa.gov.au/datacentre/datacentreDb.asp). Proterozoic basin ages are defined in Martin and Thorne (2002), Occhipinti et al. (1997) and Pirajno et al. (2004).
Figure 1

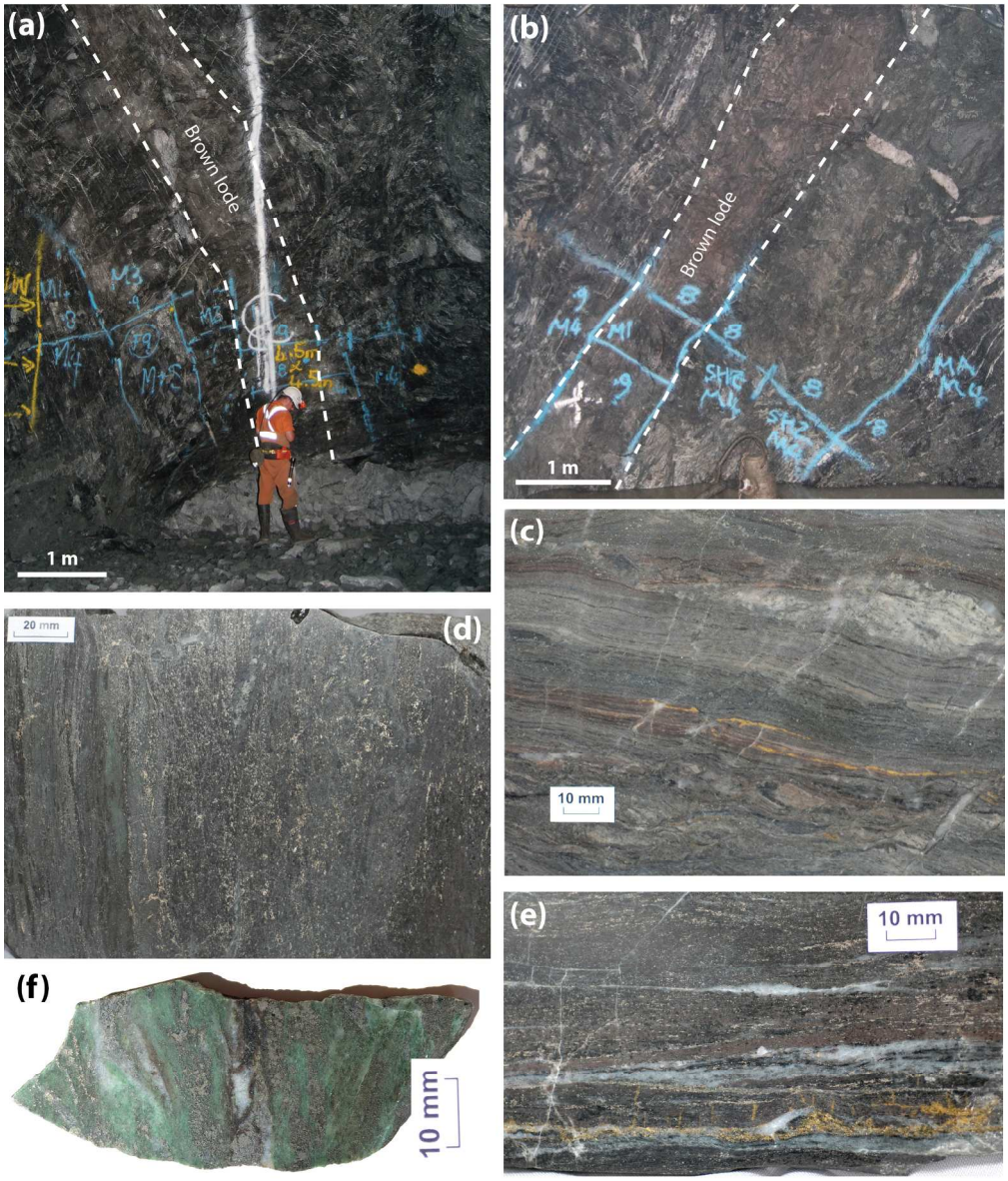

Figure 2. Representative underground and polished hand samples of mineralisation at Plutonic. (a, b) Typical brown lode in underground faces; (c) cherty lode with late-stage Au; (d) pyrrhotite-rich brown lode with abundant chlorite, (e) thin metachert with abundant late-stage Au and pyrrhotite in the more mafic wall rock, and (f) muscovite-rich green lode.
Figure 2

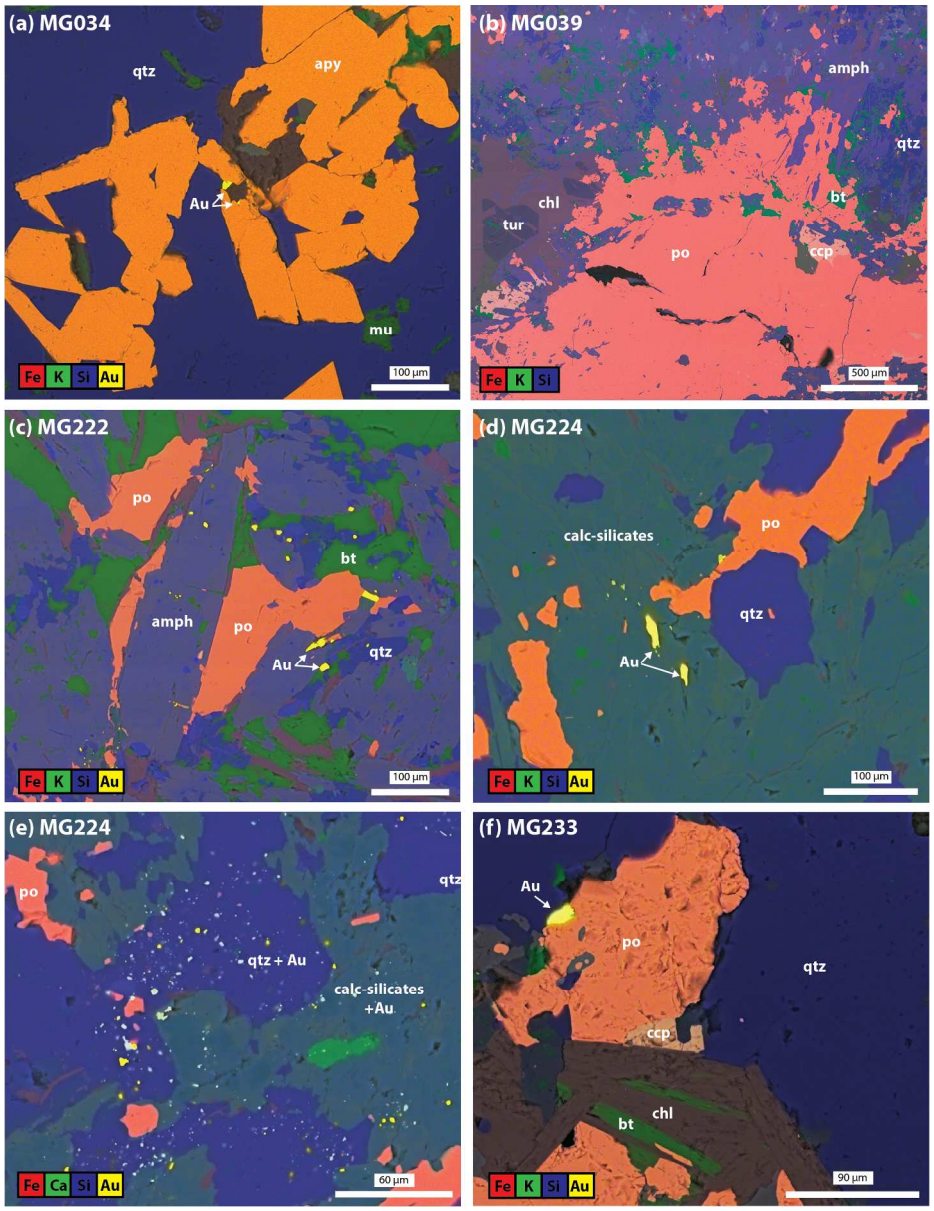

Figure 3. Representative SEM EDS maps of mineralised samples from Plutonic; mineral abbreviations after Kretz (1983); amph = amphibole. Elements included in the map as indicated. (a) MG034, muscovite-rich lode, predominantly a quartz–muscovite–arsenopyrite rock with Au associated with the boundaries of arsenopyrite grains or as inclusions therein; (b) MG039, massive pyrrhotite on the mafic–ultramafic boundary, minor chalcopyrite associated with pyrrhotite; (c–e) MG222/MG224, brown lode with late-stage pyrrhotite associated with visible Au overprinting metamorphic amphibole, Au is typically associated with biotite or calc-silicate alteration; and (f) MG233, sheared brown lode, Au is associated with pyrrhotite and may be disseminated through the quartz and calc-silicate alteration as per panel (e), biotite is commonly chloritised.
Figure 3

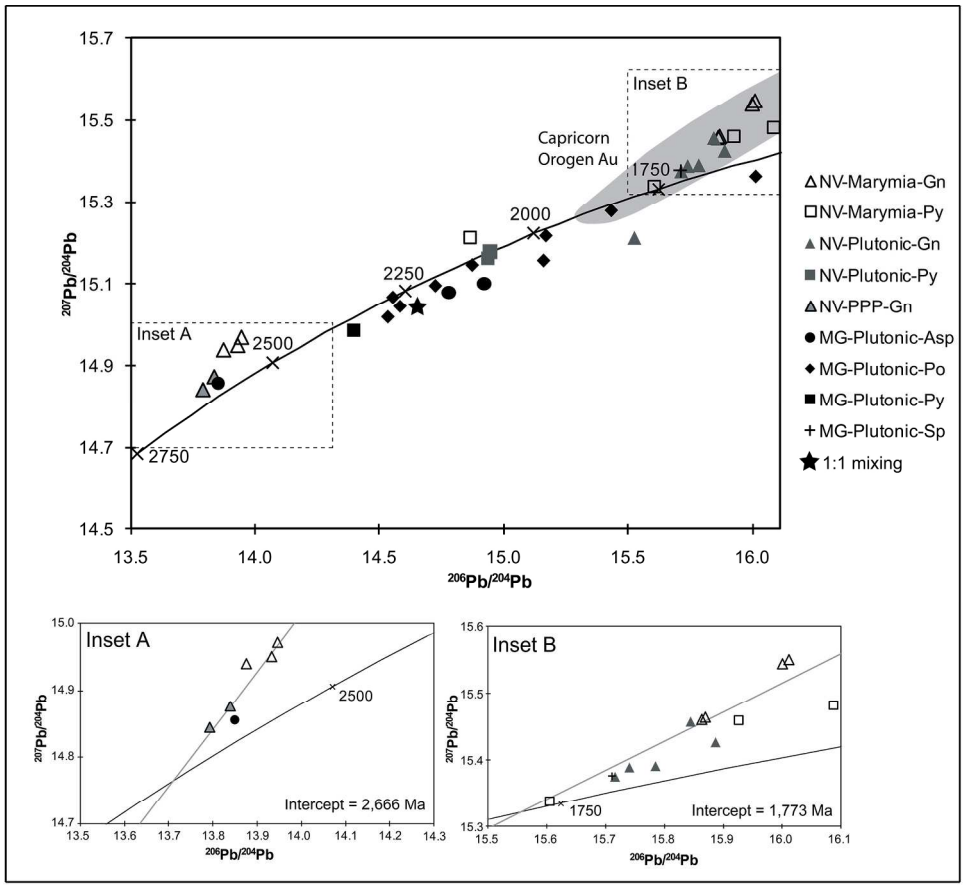

Figure 4. Concordia diagram showing 206Pb/204Pb and 207Pb/204Pb isotope ratios for sulfide minerals from the Plutonic Well Greenstone Belt from this study (MG), and Vielreicher et al. (2002) (NV). Mineral abbreviations after Kretz (1983). The grey shaded field represents Pb isotope ratios from the Peak Hill area (after Vielreicher & McNaughton, 2002, and references therein). The star indicates a theoretical Pb isotope composition derived from approximately equal proportions of sulfides that crystallised in two different events at ca 2650 and ca 1720 Ma. Location abbreviations: Marymia = Marymia Gold Mine; PPP = Triple P deposit; Plutonic = Plutonic Gold Mine.

Figure 4
203x181mm (300 x 300 DPI)

Table 1 $^{87}Rb/^{86}Sr$ and $^{87}Sr/^{86}Sr$ ratios for biotite- and muscovite-bearing samples from Plutonic.

Sample	Mineral	Mg/(Mg + Fe_T)[1]	$^{87}Rb/^{86}Sr$[2]	$^{87}Sr/^{86}Sr$[2]	Error (2σ)	Age (Ma)[3]	Initial $^{87}Sr/^{86}Sr$
MG034	Muscovite	-	6.44	0.914396	0.000032	2296 ± 99	0.7145 ± 0.0013
	Muscovite		7.40	0.941446	0.000064		
	Whole Rock		4.08	0.833367	0.000020		
MG034	Biotite	0.77–0.79	17.9	1.186878	0.000016	1779 ± 46	0.7291 ± 0.0037
	Whole Rock		4.08	0.833367	0.000020		
BCR[4]				0.705029	0.000008		
BHVO-2[5]				0.703467	0.000008		

[1]Phlogopite (Mg / (Mg + Fe_T)) composition is shown where relevant as determined by electron probe microanalyses. [2]An error of ±1% is attributed to $^{87}Rb/^{86}Sr$ ratios and 2σ error as stated for $^{87}Sr/^{86}Sr$ ratios. [3]Isochron ages were calculated using a ^{87}Rb decay constant of 1.42×10^{-11} yr^{-1} (Steiger & Jäger, 1977). [4]BCR-2 $^{87}Sr/^{86}Sr = 0.705000 \pm 0.000030$ (Jochum et al., 2005). [5]BHVO-2 $^{87}Sr/^{86}Sr = 0.703467 \pm 0.000017$ (Jochum et al., 2005).

Table 2 Lead isotope compositions of sulfides from samples from Plutonic samples.

Sample	Mineral[1]	Description	$^{208}Pb/^{204}Pb$[2]	$^{207}Pb/^{204}Pb$	$^{206}Pb/^{204}Pb$	Model age (Ma)[3]	Model age (Ma)[4]
MG801	asp	Qtz–tur–asp–Au vein	33.646	14.856	13.851	2628	2731
MG802	py	Qtz–py–Au vein	34.264	14.987	14.398	2321	2374
MG340	po	Qtz–cal–po vein	34.147	15.068	14.553	2273	2353
MG233	po	Brown lode	34.242	15.020	14.533	2250	2296
MG222	po	Brown lode	34.346	15.046	14.589	2235	2284
MG218	po	Qtz–cal–po vein	34.475	15.096	14.724	2174	2237
MG224	po	Brown lode	34.513	15.146	14.873	2110	2180
MG034	asp	Ms-rich lode	34.704	15.081	14.778	2124	2163
MG034	asp	Ms-rich lode	35.071	15.101	14.922	2039	2064
MG201	po	Bintang Fault	34.743	15.217	15.170	1962	2029
MG034	po	Ms-rich lode	34.895	15.157	15.160	1919	1942
MG025	po	Bintang Fault	35.136	15.277	15.433	1833	1900
MG800	sp	Qtz–sp vein	35.468	15.376	15.711	1730	1827
MG039	po	Ultramafic	36.339	15.361	16.015	1,516	1561

[1]All mineral abbreviations after Kretz (1983). [2]Errors on Pb isotope analyses are <0.05%. [3]Pb isotope model ages calculated with multi-stage $t_{7/6}$ evolution model of Cumming and Richards (1975) and have an error of ± 50 Myr. [4]Pb isotope model ages calculated with multi-stage $t_{7/6}$ evolution model of Stacey and Kramers (1975) and have an error of ± 50 Myr.

Table 3 Uranium and lead concentrations of sulphides from samples from Plutonic .

Sample	Mineral[1]	U (ppb)	± 1σ	Pb (ppm)	± 1σ
MG802	py	387	16.1	148.56	8.38
MG233	po	142	7.06	8.16	0.48
MG222	po	111	5.08	17.87	1.08
MG224	po	81.6	3.48	19.52	1.19
MG034	asp	41	1.87	3.85	0.21
MG201	po	0.11	0.03	6.69	0.38
MG025	po	1.57	0.22	34.2	2.01
MG039	po	1.01	0.18	9.83	0.67
MG039 dup.	po	4.09	0.46	3.79	0.25

[1]All mineral abbreviations after Kretz (1983). [2]Ratios are corrected for blank concentrations.

Table 4 Pb isotope ratios for the five most radiogenic titanite in a late-stage chlorite–carbonate vein from Plutonic.

Titanite	$^{206}Pb/^{204}Pb$	$^{207}Pb/^{206}Pb$	$^{207}Pb/^{206}Pb^{1}$	$^{207}Pb/^{206}Pb^{2}$
Crystal	Raw	Raw	NIST610 corrected	Common Pb corrected
MG354(1)	270.76	0.15607	0.15661	0.10597
MG354(2)	174.27	0.18267	0.18331	0.10450
MG354(3)	354.71	0.14354	0.14404	0.10536
MG354(8)	335.46	0.14600	0.14651	0.10563
MG354(9)	407.03	0.13965	0.14014	0.10648
			Average	0.10559
			Age	1725 ± 26 Ma

[1] $^{207}Pb/^{206}Pb$ ratios are corrected for fractionation using the NIST610 standard. [2] Common Pb correction calculated using counts of ^{204}Pb measured and $^{206}Pb/^{204}Pb$ = 15.5 and $^{207}Pb/^{204}Pb$ = 15.5 (Cumming & Richards 1975).

Table 5 Lead isotope compositions of sulfides from the PWGB.[1]

Sample	Mineral[2]	$^{208}Pb/^{204}Pb$[3]	$^{207}Pb/^{204}Pb$	$^{206}Pb/^{204}Pb$	Model age (Ma)[4]	Model age (Ma)[5]
Marymia	gn	33.639	14.937	13.874	2670	2831
Marymia	gn	33.762	14.968	13.946	2639	2801
Marymia	gn	33.684	14.948	13.931	2636	2787
Marymia	gn	34.861	15.458	15.863	1698	1831
Marymia	gn	34.964	15.461	15.869	1697	1830
Marymia	gn	35.828	15.549	16.011	1677	1850
Marymia	gn	35.813	15.541	16.000	1658	1847
Marymia	py	34.395	15.214	14.865	2169	2289
Marymia	py	35.396	15.337	15.605	1767	1852
Marymia	py	35.656	15.459	15.926	1658	1784
Marymia	py	35.570	15.482	16.087	1573	1695
Triple P	gn	33.603	14.840	13.792	2660	2770
Triple P	gn	33.677	14.872	13.837	2650	2771
Plutonic	gn	35.465	15.374	15.714	1726	1821
Plutonic	gn	35.495	15.387	15.740	1720	1820
Plutonic	gn	34.919	15.455	15.844	1708	1841
Plutonic	gn	35.470	15.389	15.784	1692	1788
Plutonic	gn	35.643	15.424	15.887	1654	1761
Plutonic	py	34.853	15.163	14.937	2079	2149
Plutonic	py	34.377	15.178	14.945	2085	2165

[1]Analyses from Vielreicher *et al*. (2002) and references therein. Data are reproduced here for convenience. [2] gn = galena; py = pyrite. [3]Errors on Pb isotope analyses are ± 0.15%. [4]Pb isotope model ages calculated with multi-stage $t_{7/6}$ evolution model of Cumming and Richards (1975) and have an error of ± 30 Myr (Vielreicher *et al*. 2002). [5]Pb isotope model ages calculated with multi-stage $t_{7/6}$ evolution model of Stacey and Kramers (1975)